NJC

PAPER

View Article Online
View Journal | View Issue

Cite this: *New J. Chem.*, 2016, **40**, 2710

Physicochemical and antimicrobial photodynamic chemotherapy of unsymmetrical indium phthalocyanines alone or in the presence of magnetic nanoparticles†

Olawale L. Osifeko,[a] Imran Uddin,[b] Philani N. Mashazi[a] and Tebello Nyokong*[a]

Received (in Montpellier, France) 22nd July 2015,
Accepted 19th January 2016

DOI: 10.1039/c5nj01922b

www.rsc.org/njc

An AB_3 type photosensitiser, consisting of 4-pyridylsulfanyl units (denoted as B_3) and one aminophenoxy (denoted as A) group (complex **3**) was synthesized. Complex **3** was then quaternized to form complex **4**. The aminophenoxy substituent of complex **3** was used for the formation of the amide linkage with the carboxylic functionalised magnetic nanoparticles. Complexes **3** and **4** and their conjugates with magnetic nanoparticles were then used for photodynamic antimicrobial chemotherapy on *E. coli*. The cationic photosensitiser **4** showed a high efficiency for photodynamic antimicrobial chemotherapy at a very low concentration compared to its conjugate on *E. coli*.

Introduction

Photodynamic antimicrobial therapy (PACT) is based on the administration of a photosensitizer, which is selectively localized in microbial cells. Upon irradiation with light of appropriate wavelength, the photosensitizer produces singlet oxygen that is cytotoxic to the targeted bacteria.[1,2]

Phthalocyanine (Pc) derivatives have gained significance in a number of fields including their use as photosensitizers in photodynamic therapy (PDT) of cancer.[3,4] Pcs are efficient photosensitizers for both PACT[5] and PDT due to their ability to absorb visible light, becoming excited to the triplet state, and then transferring the energy to molecular oxygen to form cytotoxic singlet oxygen.[6] The Pcs' wide range of applications are related to the possibility of varying the Pc structure and, consequently, the electronic configuration in a controlled fashion through peripheral substitution, variation of the central atom, or changes in the axial ligand.[7–9] In this work, a Pc will be linked to magnetic nanoparticles (MNPs) for PACT.

The important properties of magnetic nanoparticles for medical applications are nontoxicity, biocompatibility, injectability, and high-level accumulation in the target tissue or organ.[10] Magnetic nanoparticles have potential for use in various fields such as magnetic resonance imaging (MRI), hyperthermia, drug delivery and cell separation.[11–14] The surface of magnetic nanoparticles can be functionalized to allow for attachment to other compounds to produce bifunctional nanocomposites.[15] Linking of phthalocyanines to MNPs allows for possible MRI and PDT applications.[16]

The goal of this work is to explore the photodynamic antimicrobial chemotherapy activity of a low symmetry phthalocyanine {9(10), 16(17), 23(24)-tri-4-pyridylsulfanyl-2(3)-(4-aminophenoxy)-phthalocyaninato chloroindium(III), complex **3**, Scheme 1} when conjugated to carboxylic acid functionalized Fe_3O_4 magnetic nanoparticles (MNP-COOH). The photochemical/photophysical parameters of the conjugates will also be discussed. Cationic photosensitizers have been reported to be more effective than their anionic and neutral counterparts against Gram (−) bacteria, such as *E. coli*.[6] The outer membrane of Gram (−) bacteria is made up of a negatively charged layer which becomes impermeable to neutral and negatively charged photosensitizers, hence positively charged photosensitizers are more active for Gram (−) bacteria.[17] Thus cationic (quaternized) indium phthalocyanine is employed in this work. We chose indium as a central metal since it is a heavy atom. The presence of In will enhance intersystem crossing to the triplet state which will subsequently lead to high singlet oxygen quantum yields. The presence of sulphur bridges in complex **3** will shift the Q band to the biological window[18] hence improving PACT activity. The low symmetry InPc is employed since asymmetrical Pcs have shown improved PACT activity.[19] Recently we reported on the photodynamic antimicrobial effect of low symmetry indium pyridyloxy phthalocyanine with only one quartenizable group which limited water solubility.[20] Complex **3** has more quartenizable groups which will enhance water solubility.

Ag and Au nanoparticles have been linked to phthalocyanines with improved PACT activity.[21,22] This work reports for the first time on the combination of Pcs and MNPs for PACT.

[a] *Rhodes University, Department of Chemistry, Grahamstown, South Africa. E-mail: t.nyokong@ru.ac.za*
[b] *National Chemical Laboratory, Biochemical Sciences Division, Pune, India*

† Electronic supplementary information (ESI) available. See DOI: 10.1039/c5nj01922b

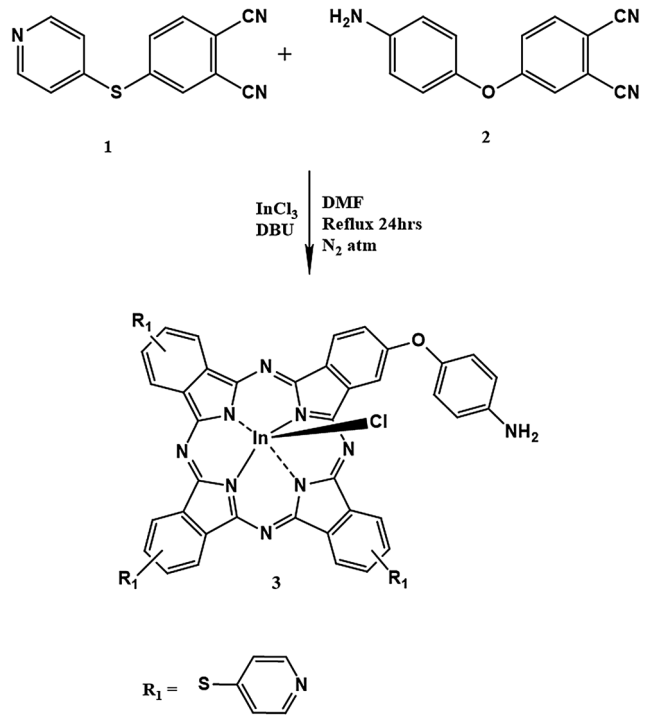

Scheme 1 Schematic representation of the synthesis of **3**.

MPcs have been linked to MNPs for photophysical and photochemical studies,[23–25] but not for PACT. The MPcs employed in literature were symmetrically substituted. Asymmetric MPc containing one group for linking to MNPs are preferred since there is more defined coordination. This work reports on the first example of such a molecule for linkage to MNPs. The main advantage of the use of the MNPs is the ability to remove the conjugated photosensitiser using a magnet allowing for pure separation of the conjugate following PACT.

The Pc is linked to the MNPs by taking advantage of the amino groups on the Pc and the carboxylic group provided by the carboxylic acid functionalized magnetic nanoparticles (MNP-COOH) for the formation of an amide bond.

Experimental

Materials

Indium(III) chloride, absolute ethanol (EtOH), 3-aminopropyltriethoxysilane (APTES), tetraethoxysilane (TEOS), succinic anhydride, dicyclohexylcarbodiimide (DCC), spectroscopic dimethyl formamide (DMF), dimethyl sulfoxide (DMSO), zinc phthalocyanine (ZnPc), anthracene-9,10-bis-methylmalonate (ADMA), 1,3-diphenylisobenzofuran (DPBF), iron(III) chloride hexahydrate, iron(II) sulphate tetrahydrate, 1,8-diazabicycloundec-7-ene (DBU) and methyl iodide were purchased from Sigma-Aldrich. Deuterated dimethyl sulfoxide (DMSO-d_6) and aqueous ammonia (25 wt%), were purchased from SAARCHEM. Agar bacteriological BBL Muller Hinton broth and nutrient agar were purchased from Merck. *Escherichia coli* (ATCC 25922) was purchased from Microbiologic; Phosphate buffer saline (10 mM PBS) pH 7.4 buffer was prepared using appropriate amounts of Na_2HPO_4, KH_2PO_4 and chloride salts using ultrapure water from a Milli-Q Water System (Millipore Corp, Bedford, MA, USA). 4-Pyridylsulfanyl phthalonitrile (**1**) and 4-aminophenoxyphthalonitrile (**2**) (Scheme 1) were synthesized according to reported procedures.[26–28] AlPcSmix (containing a mixture of sulfonated derivatives) was synthesized according to literature methods[29] and used as a standard for singlet oxygen determination in aqueous media.

Equipment

Transmission electron microscopy (TEM) images were obtained using a ZEISS LIBRA® transmission electron microscope. Ultraviolet-visible (UV-Vis) absorption spectra were recorded on a Shimadzu UV-2550 spectrophotometer. Infrared (IR) spectra were recorded on a Perkin-Elmer Fourier transform-IR (100 FT-IR) spectrophotometer. Fluorescence emission spectra were recorded on a Varian Eclipse spectrofluorimeter.

Irradiations for singlet oxygen and photodegradation quantum yield determinations as well as antimicrobial studies were performed using a General Electric Quartz lamp (300 W), 600 nm glass (Schott) and water filters were used to filter off ultraviolet and far infrared radiations respectively. An interference filter, 700 nm with a band of 40 nm, was placed in the light path just before the cell containing the sample. Light intensities were measured with a POWER MAX 5100 (Molelectron detector incorporated) power meter and were found to be 3.8×10^{16} photons cm^{-2} s^{-1}. Mass spectral data were collected with a Bruker AutoFLEX III Smartbeam TOF/TOF Mass spectrometer. The spectra were acquired using dithranol as the MALDI matrix. ^1H nuclear magnetic resonance spectra were recorded on a Bruker AMX 600 MHz NMR spectrometer.

Thermo-gravimetric analysis (TGA) was performed using a Perkin Elmer TGA 4000 analyzer. The analysis was carried out under nitrogen at a flow rate of 20 mL min^{-1}. The weighed sample masses were heated from 50 to 800 °C at a heating rate of 10 °C min^{-1}.

X-ray diffraction (XRD) analysis was performed on a Bruker D8 Discover diffractometer, equipped with a Lynx Eye detector, under Cu-K_α radiation (λ = 1.5405 Å). Data were collected in the range from $2\theta = 10^\circ$ to 100°, scanning at 0.010° min^{-1} and 192 s per step. The samples were placed on a zero background silicon wafer slide.

Fluorescence decay times were measured using a time correlated single photon counting (TCSPC) setup (FluoTime 300, Picoquant GmbH). The excitation source was a diode laser (LDH-P-670 driven by PDL 800-B, 670 nm, 20 MHz repetition rate, 44 ps pulse width, Pico quant GmbH).

Laser flash photolysis system was used for the determination of triplet decay kinetics. Details of the equipment have been provided before.[24] For laser flash photolysis studies, the absorbance of solutions of the Pcs and the ZnPc standard was ~1.5 at the Q band. The solution was introduced into a 1 cm path length UV-visible spectrophotometric cell and de-aerated using argon for 15 min.

X-ray photoelectron spectroscopy (XPS) analysis was done using an AXIS Ultra DLD, with Al (monochromatic) anode equipped with a charge neutraliser, supplied by Kratos Analytical. The following parameters were used: the emission was 10 mA, the anode (HT) was 15 kV and the operating pressure below 5×10^{-9} torr. A hybrid lens was used and resolution to acquire scans was at 160 eV pass energy in slot mode. The centre used for the scans was at 520 eV with a width of 1205 eV, with steps at 1 eV and dwell time at 100 ms as reported before.[30] The high resolution scans were acquires using 80 eV pass energy in slot mode.

Nitrogen adsorption/desorption isotherms were measured at 77 K using a Micrometrics ASAP 2020 Surface Area and Porosity Analyzer. Prior to each measurement, degassing was carried at 90 °C for four days. The Brunauer–Emmett–Teller (BET) method was employed to determine surface area and porosity. The BET surface area and total pore volume were calculated from the isotherms obtained. The details of the set-up have been previously described.[30] The optical density of the bacteria culture were determined using the LEDETECT 96 from LABXIM PRODUCTS. Vortex mixer and HERMLE Z233M-2 centrifuge from LASIEC were used to mix the bacteria suspension and for the harvesting of the bacteria cells, respectively.

Antimicrobial studies

Preparation of bacterial culture. The bacteria culture was prepared according to the procedure described previously by us.[20] Briefly aliquots of the culture were aseptically transferred to 4 mL of fresh broth and incubated at 37 °C to mid logarithmic phase (absorbance ≈ 0.6 at 620 nm). The bacteria culture in the logarithmic phase of growth were harvested through the removal of broth culture by centrifugation (3000 RPM for 15 min), washed once with 10 mM of PBS and re-suspended in 4 mL of PBS. Then the bacteria culture was diluted to 1/1000 in PBS (working stock solution), corresponding to $\approx 10^8$ colony forming units (CFU) per mL.[31]

Photodynamic antimicrobial chemotherapy activity. Photodynamic antimicrobial chemotherapy study of the *E. coli* was performed using methods previously reported[20,32,33] using 0.43% to 1.8% DMSO in PBS. In all the experiments, the *E. coli* suspension were incubated in an oven equipped with a shaker for 30 min in the dark at 37 °C. Then half (1 mL) of the incubated *E. coli* suspensions were irradiated at the Q-band maximum of the photosensitizers in 24 well plate, using the set-up described above at different time intervals, while the other half was kept in the dark. After irradiation 100 μL samples were serially diluted (10 fold) with PBS and were aseptically spotted on agar plates using micropipette.[34] The plates were incubated inverted at 37 °C overnight for 24 h. The absorbance of the cell suspension were measured before and after incubation for 30 min (this has been reported to result in localization of the photosensitizer within the cytoplasm of the bacteria[35]) then finally after 60 min of photoinactivation experiments.

Statistical analysis. All experiments were done in triplicate. Statistical significance (p value) was determined using Anova (analysis of variance) and a Student's t-test (analysis between two components) using error limits from at least three determinations. The analysis of variance for photoinactivation effect of the photosensitizers were determined at the highest fluence at which comparisons could be made[36] and p-value < 0.05 was considered significant.

Synthesis of MNPs

Bare MNPs (Scheme 2). The magnetite nanoparticles were prepared by the conventional co-precipitation method, using previously reported procedures[37,38] with some modifications. Briefly 4.17 g (25.70 mmol) of iron(III) chloride hexahydrate and 1.95 g (12.84 mmol) of iron(II) sulphate tetrahydrate ($FeSO_4 \cdot 4H_2O$) were dissolved in 80 mL of previously degassed Millipore water under nitrogen gas. Then 7.5 mL of liquid ammonia (25%) was added drop-wise. The mixture was stirred for 3 h in an argon atmosphere at the temperature of 60 °C. Following this, the slurry was washed repeatedly with distilled water and the particles were magnetically separated from the supernatant and re-dispersed in aqueous solution at least three times, until pH 7 was obtained. The MNPs were then finally dispersed in ethanol, magnetically isolated and dried in vacuum at room temperature. The dried bare magnetic nanoparticles are represented as MNPs, Scheme 2.

Silica coated magnetic nanoparticles (MNP-Si), Scheme 2. The bare MNPs surface were encapsulated with silica for easy functionalization as follows: MNPs (0.26 g) were dispersed in a degassed mixture of 80 mL absolute ethanol and water, followed by ultrasonication of the mixture for 30 min. Then, 5 mL of tetraethoxysilane (TEOS) was added to the mixture and pH was adjusted to 9 using ammonium hydroxide. The mixture was stirred in an inert argon environment for 12 h. This was followed by refluxing at 130 °C for 24 h. The brown precipitate was separated and dried and is represented as MNP-Si in Scheme 2. IR [(ATR), τ_{max}/cm^{-1}]: 3234 (O–H), 2160, 1055 (Si–O–Si), 951 (Si–OH), 797.

Amino coated magnetic nanoparticles (MNP-NH_2, Scheme 2). The silica coated magnetic nanoparticle (0.15 g) and 100 mL absolute ethanol were ultrasonicated for 30 min in order to form homogeneous colloid suspension. Then 0.5 mL APTES was added and the mixture heated under reflux in a nitrogen atmosphere at 130 °C for 7 h. The precipitate was separated magnetically. The resulting solid product (represented as MNP-NH_2, Scheme 2), was washed with distilled water and dried in the vacuum for 24 h. IR [(ATR), τ_{max}/cm^{-1}]: 3282 (N–H), 1065 (Si–O–Si), 794 (N–H).

Carboxylic acid functionalized magnetic nanoparticles (MNP-COOH, Scheme 2). To a stirring solution of succinic anhydride (0.1 M, 20 mL) in dry DMF, the dispersed solution of MNP-NH_2 (0.1 g) in dry DMF was added dropwise. The mixture was stirred for 24 h then poured into absolute ethanol. The MNP-COOH were magnetically separated, washed several times with absolute ethanol and dried under vacuum. IR [(ATR), τ_{max}/cm^{-1}]: 3215 (–COOH), 2160, 1646, 1058 (Si–O–Si), 796.

Synthesis of phthalocyanines and conjugates

9(10),16(17),23(24)-Tri-4-pyridylsulfanyl-2(3)-(4-aminophenoxy) phthalocyaninato chloroindium(III) (3). A mixture of 4-aminophenoxy phthalonitrile (**2**, 0.06 g, 0.23 mmol), 4-pyridylsulfanyl

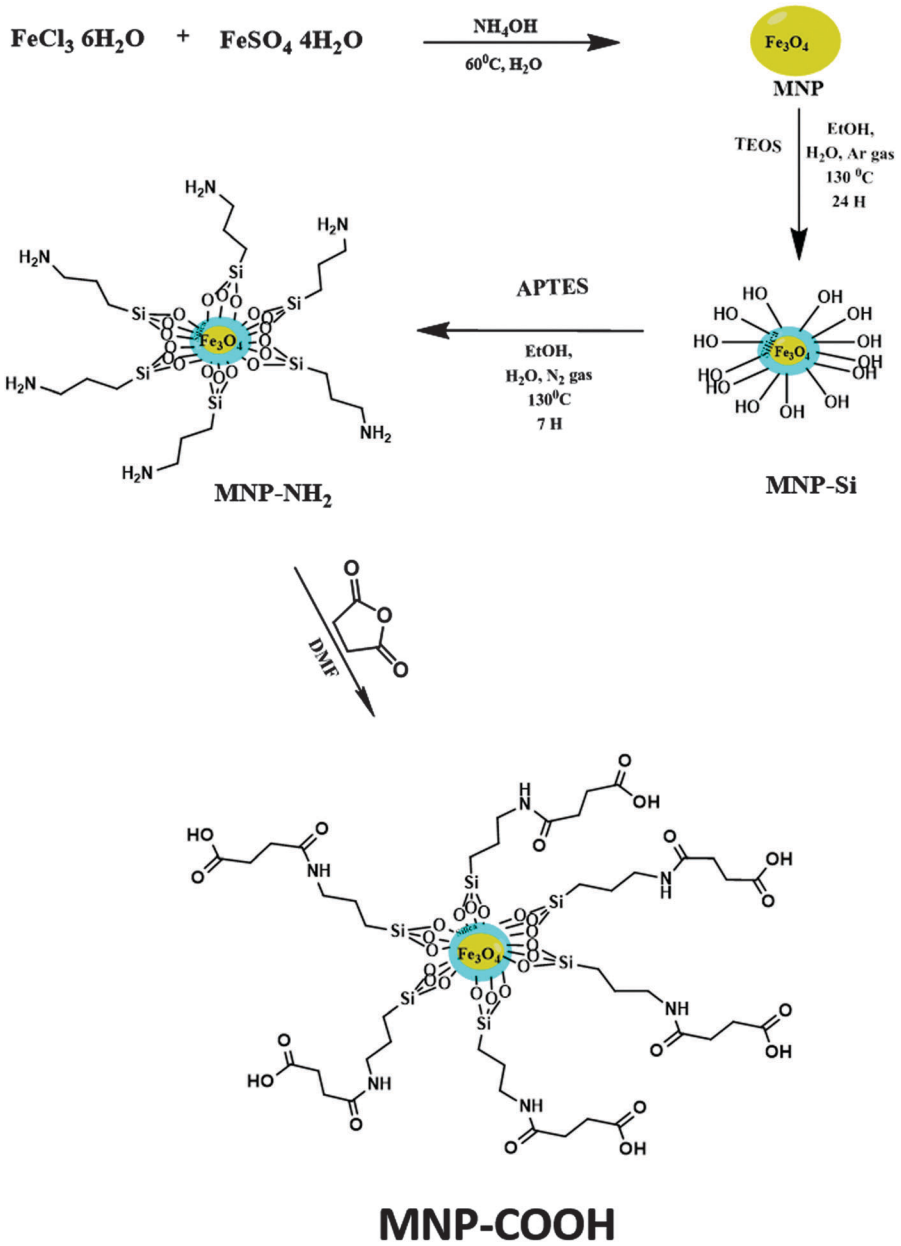

Scheme 2 The scheme for the synthesis of bare MNP, MNP-Si, MNP-NH_2 and MNP-COOH.

phthalonitrile (**1**, 0.17 g, 0.70 mmol), In(III) chloride (0.05 g, 0.23 mmol) and 0.5 mL DBU in 5 mL of *n*-pentanol was heated at reflux temperature under an argon atmosphere for 24 h with constant stirring. The product obtained was precipitated with methanol and subsequently washed with water and dried in the oven. The filtered crude product was purified *via* Soxhlet extractor for 4 days using absolute ethanol then the dried extract was further subjected to column chromatography using dichloromethane (DCM)/methanol (95 : 5).

Yield: 0.16 g (63.4%). IR [(ATR), ν_{max}/cm^{-1}]: 3332(N–H), 1723, 1666, 1597, 1480, 1385, 1330, 1225 (C–O–C), 1064, 1011, 910, 813. ^{1}H NMR (DMSO-d_6): δ {ppm} 6.64–6.62 (s, 2H, NH_2–H), 6.88–6.86 (s, 4H, Pc–H), 7.26–7.23 (dd, 7H, J = 4.8, 1.4 Hz; phenyl-H and Pc–H), 7.85–7.83 (s, 3H, Pc–H), 7.91–7.89 (d, 6H, J = 2.5 Hz, pyridyl-H), 8.44–8.48 (dd, 8H, J = 4.7, 1.3 Hz; pyridyl-H and Pc–H). ^{13}C NMR (DMSO-d_6): δ {ppm} 122.92 (aromatic phenyl-CH), 124.59 (aromatic pyridyl-CH), 126.74 (aromatic C), 132.74, 134.32, 138.16, 138.44 (aromatic C), 146.26 (aromatic phenyl-CH), 150.12 (aromatic pyridyl-C=N), 150.27, 162.62 (aromatic Pc–C), 168.57 (aromatic Pc–C), 168.73 (aromatic Pc–C).

UV/Vis (DMSO) λ_{max} nm (log ε): 696 (5.22), 628 (4.57), 369 (4.93). Calcd. for $C_{53}H_{30}ClInN_{12}OS_3$: expected: C 58.01, H 2.76, N 15.32, found: C 58.79, H 2.53, N 15.68. MALDI TOF MS *m*/*z*: calcd: 1097, found: $[M + 3H]^+$ = 1100.

Cationic 9(10),16(17),23(24)-tri-*N*-methyl-4-pyridylsulfanyl-2(3)-(4-aminophenoxy)phthalocyaninato chloroindium(III) triiodide (4). Complex **4** (quaternation of **3**) was synthesized by refluxing a

mixture of complex **3** (106 mg, 0.10 mmol), methyl iodide (1.0 mL), DMF (10 mL) and acetone (20 mL) for 48 h. The reaction mixture was cooled to room temperature and precipitated with diethyl ether and washed with acetone then oven dried.

Yield: 68.9 mg (65%). IR [(ATR), ν_{max}/cm^{-1}]: 3403 (N–H stretch), 3020 (C–H), 1714, 1626 (N–H bend), 1488, 1383, 1326, 1304, 1226, 1138, 1088, 1041 (C–O–C), 908. ^{1}H NMR (DMSO-d_6): δ {ppm} 4.38–4.12 (S, 9H methyl-H), 6.78–9.92 (br, 30H Ar–H and NH_2–H). UV/Vis (DMSO) λ_{max} nm ($\log\varepsilon$): 698 (4.89), 629 (4.28), 368 (4.63). Calcd. for $C_{56}H_{39}ClI_3InN_{12}OS_3$: C 44.16, H 2.58, N 11.03, found: C 44.68, H 2.86, N 10.07. MALDI TOF MS *m*/*z*: calcd: 1523.17; found: (1) [M − $3I^-$, −3H] = 1140, (2) [M − Cl, $+CH_4I^+$, $-Cl^-$] = 1244 and (3) [M − Cl^-, −8H] = 1480.

9(10),16(17),23(24)-Tri-4-pyridylsulfanyl-2(3)-(4 aminophenoxy)-phthalocyaninato chloroindium(III)–Fe_3O_4 nanoparticles conjugates (3-MNPs, Scheme 3). The conjugate was synthesised in accordance to previously reported procedure within our group.[39] A mixture of 0.10 g of MNP-COOH and 0.02 g (0.097 mmol) DCC was stirred in 4 mL DMF at room temperature for 48 h. Compound **3** (0.10 g, 0.091 mmol) dissolved in 2 mL DMF was added dropwise to the mixture, and stirring continued for a further 48 h. The crude product was collected and washed several times by centrifugation in acetone, methanol and absolute ethanol in succession to remove DMF, unbound complex **3** and excess DCC. The dry nanocomposite (**3**-MNPs) was obtained by oven drying at 110 °C for 48 h. Yield: 0.12 g. IR [(ATR), τ_{max}/cm^{-1}]: 3064 (–COOH), 1725, 1599, 1572 (N–H bend), 1479, 1330, 1064 (Si–O–Si), 909.

9(10),16(17),23(24)-Tri-*N*-methyl-4-pyridylsulfanyl-2(3)-(4-amino-phenoxy)phthalocyaninato chloroindium(III) triiodide–Fe_3O_4 nanoparticles conjugates (4-MNPs). **4**-MNPs was synthesized following literature methods for quaternized porphyrin magnetic nanoparticle conjugates.[40] **3**-MNPs (0.075 g) was dissolved in a solvent mixture of 2 mL of DMF and 10 mL of acetone. Then 1 mL of methyl iodide was added to the flask and the mixture heated at reflux at 40 °C for 48 h. The reaction mixture was cooled to room temperature (~25 °C) and precipitated with diethyl ether and

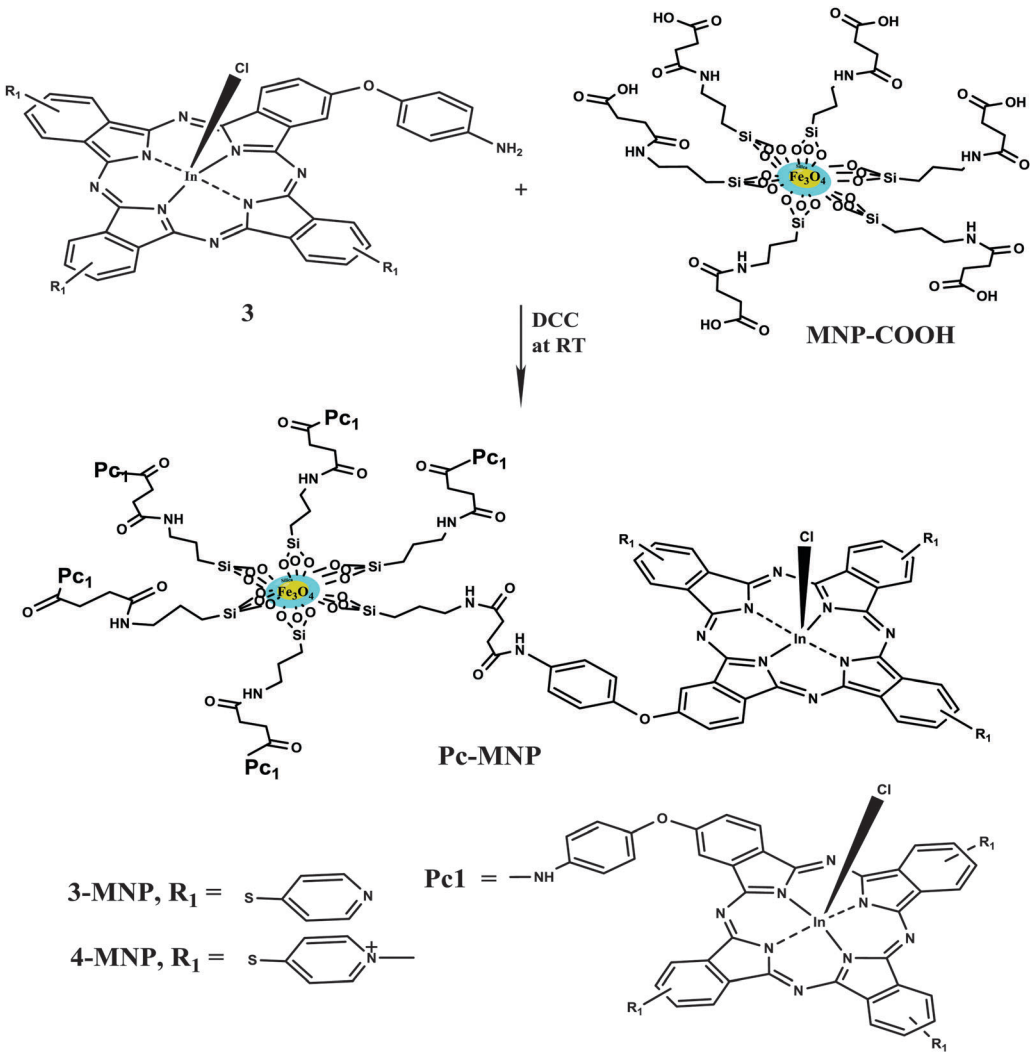

Scheme 3 Schematic representation of the conjugation of MNP-COOH and the photosensitisers (**3** and **4**).

washed with acetone then oven dried. Yield: 0.052 g. IR [(ATR), ν_{max}/cm^{-1}]: 3060 (–COOH), 1630 (N–H bend), 1472, 1036 (Si–O–Si).

Result and discussion

Synthesis and characterization of complexes 3 and 4

Compound **3** was produced by template cyclization of 4-aminophenoxy phthalonitrile (**2**) and 4-pyridylsulfanyl phthalonitrile (**1**) in the presence of $InCl_3$ in an inert atmosphere using DMF as the reaction medium (Scheme 1). Compound **4** was obtained *via* quaternization of compound **3** using methyl iodide as the quaternizing agent. Both complexes were characterized by elemental analysis and several spectroscopic techniques. The elemental analyses gave percentage carbon values that were within 1% in all cases, which are within acceptable for phthalocyanine complexes.

^{1}H NMR spectrum of **3** (Fig. S1, ESI†) provided the characteristic chemical shifts for the structure expected. ^{1}H NMR spectrum of the **3** exhibited the aromatic protons at δ = 8.44–8.48 ppm and δ = 7.26–7.23 ppm as doublet of doublets, and δ = 7.91–7.89 ppm as a doublet. NH_2 protons were observed as a singlet at δ = 6.64–6.62 ppm and other aromatic protons were observed at δ = 6.88–6.86 ppm and δ = 7.85–7.83 ppm respectively.

Strong COSY correlations (Fig. S2, ESI†) were observed between the two doublet of doublet; phenyl-H resonance at 7.26–7.23 (dd, 7H, J = 4.8, 1.4 Hz; phenyl-H and Pc–H) and pyridyl-H at 8.44–8.48 (dd, 8H, J = 4.7, 1.3 Hz; pyridyl-H and Pc–H). The signals along the diagonal reflect the normal ^{1}H–^{1}H spectrum. ^{13}C NMR spectrum (Fig. S3, ESI†) showed typical aromatic carbons between 120–170 ppm. Mass spectrum for complex **3** is shown in Fig. S4A (ESI†) and is consistent with the complex. For complex **4**, quaternization of the pyridyl nitrogen is well known. It also possible to methylate the NH_2 groups, with eventual quaternization. XPS (to be discussed below) shows the presence of NH for **4**, hence does not support full quaternization of the NH_2. We could not find evidence in literature for the quaternization of NH_2 substituted Pcs using methyl iodide. There have been reports of the formation of $NH_3^+Cl^-$ when an amino substituted Pc is reacted with hydrochloric acid.[41] The ^{1}H NMR spectrum for **4** showed a broad integration which could not be assigned to a particular peak, but there is a clear presence of the alkyl group up field, Fig. S5 (ESI†). The expected number of aromatic is 28, but the observed number of protons in the aromatic area is 30, due to the presence of the overlapping NH_2 peaks. The mass spectral data for **4** showed three prominent peaks which are assigned to (i) removal of $3I^-$ and $3H^+$ (1140 g), (ii) removal of $6H^+$ and displacement of Cl^- by $CH4I^+$ (1244 g) (iii) removal of Cl^- and $8H^+$ (1480), see Fig. S4B (ESI†).

The UV-Vis spectra of complexes **3** and **4** are shown in Fig. 1. The Q band for **3** is observed at 698 nm and does not change significantly on quaternization to form **4**, Table 1. Complex **4** is water soluble, but highly aggregated, Fig. 1B (curve d). Addition of Triton X 100 reduces the aggregation significantly. The UV absorption of both complexes in DMSO shows monomeric behaviour.

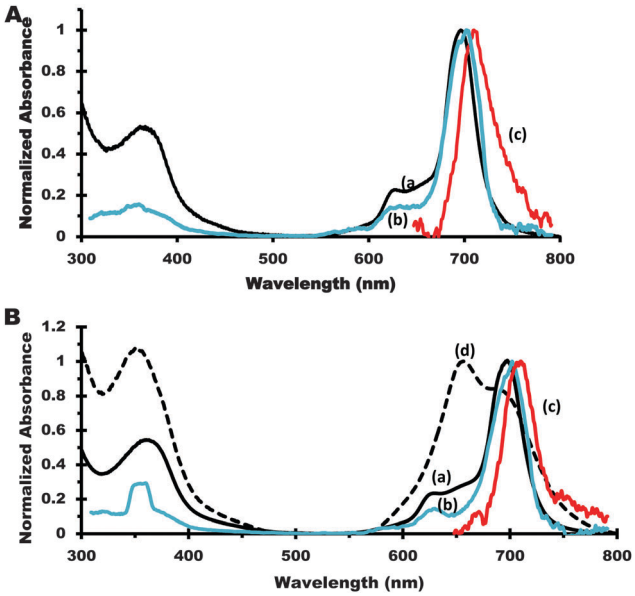

Fig. 1 Electronic absorption (a), excitation (b) and emission (c) spectra of **3** (A) in DMSO (concentration = 2.0 × 10^{-6} M) and **4** (B) in water plus Triton-X. (d) in (B) is the absorption spectrum of **4** in water.

Emission spectra were mirror images of the excitation spectra in DMSO (for **3** and **4**) or in water plus Triton X 100 (for complex **4**), Fig. 1. Slight shifts between the absorption and excitation spectra could be due to the differences in the equipment used.

Characterization of MNPs

TEM images. MNP-NH_2 and MNP-COOH were synthesized as reported before[39] except that in the current work, the isolation of the nanoparticles was done by magnetic decantation. Scheme 2 shows the synthetic route for the MNP-COOH.

The TEM images of the MNPs (Fig. 2) reveal the morphology of the MNPs at each stages of synthesis. The size distribution of the nanoparticles is shown in histograms with average diameter ranging from 10.20 nm to 20.90 nm. The MNPs are essentially spherical. The image in Fig. 2C shows increased aggregation upon functionalization with succinic anhydride (Scheme 2) to form MNP-COOH.

XRD patterns. The XRD diffractograms (Fig. 3A), show peaks characteristic of magnetite at (220), (311), (400), (422), (511) and (440), this revealed that the magnetic particles were pure Fe_3O_4 with spinel structure.

Surface area and porosity analyses. Brunauer–Emmette–Teller (BET) surface area and pore volumes of the silica and carboxylic acid coated MNPs were determined. Nitrogen adsorption–desorption isotherms for the magnetic nanoparticles and carboxylic acid functionalised MNPs are shown in Fig. 4. BET characterization show type IV sorption isotherms with surface area 56.49 m^2 g^{-1} and pore size 99.99 Å for MNP-Si. There is reduction in surface area and increase in pore size for MNP-COOH to 25.77 m^2 g^{-1} and 284.24 Å, respectively. It has been documented that a rough surface results in larger surface area than a smooth one.[42] Thus BET studies confirm that MNP-Si is rougher than MNP-COOH.

Table 1 Photophysical properties of indium(III) phthalocyanines and their conjugates in DMSO unless otherwise stated

Comp	λ_{abs} [a] (nm)	λ_{emm} [a] (nm)	λ_{exc} [a] (nm)	Φ_F	τ_F (ns)	Φ_T	Φ_Δ	Φ_{IC}	τ_T (μS)	Φ_{Pd} 10^{-5}	S_Δ
3	698	710	702	0.008	0.26	0.74	0.44	0.25	55	1.22	0.60
4	699	711	703	0.013	0.33	0.48	0.26	0.51	66	1.88	0.51
	697[b]	710[b]	702[b]	0.018[b]	0.33[b]	—	0.31[b]	—	—	13.20[b]	—
3-MNPs	699	706	705	0.013	0.24	0.53	0.35	0.46	56	1.34	0.66
4-MNPs	699	715	711	0.009	0.24	0.69	0.31	0.30	67	4.22	0.44

[a] λ_{abs} = absorption wavelength, λ_{emm} = emission wavelength and λ_{exc} = excitation wavelength. [b] In water/Triton-X 100.

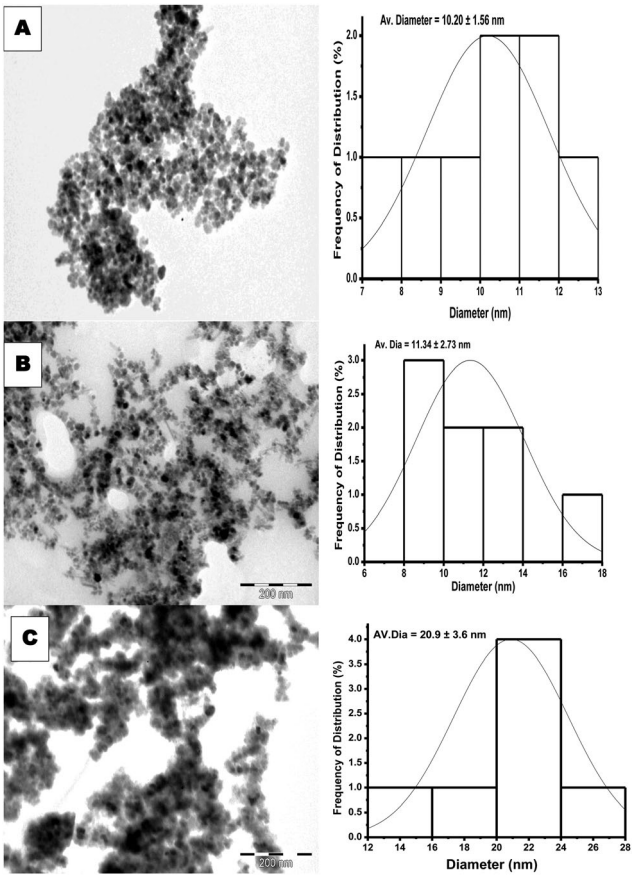

Fig. 2 TEM images and the corresponding histograms showing in (A) MNP-Si, (B) MNP-NH_2 and (C) MNP-COOH.

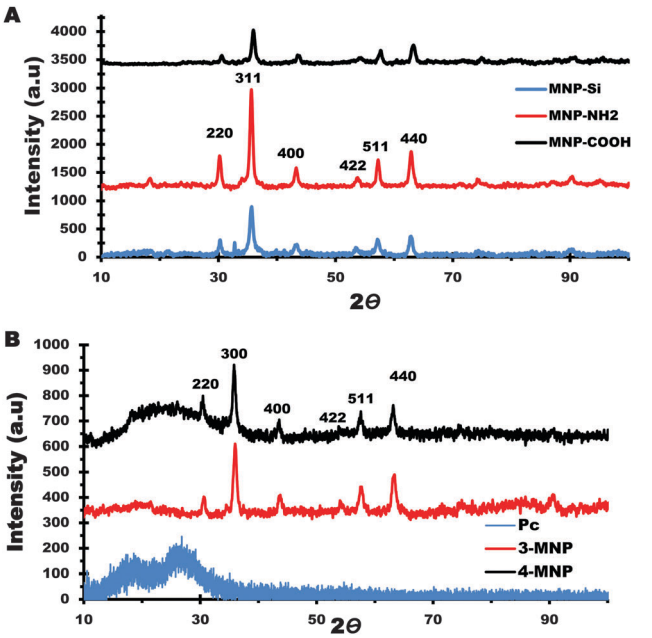

Fig. 3 Powder XRD diffractograms of (A) MNP, MNP-Si, MNP-NH_2 and MNP-COOH and (B) complex **3**, **3**-MNPs and **4**-MNPs.

Characterization of conjugates of complexes 3 and 4 with MNPs

Fig. 5 shows a photograph of the magnetic isolation process of **3**-MNPs as opposed to **3**, showing the effect of magnetic separation. MNP-COOH was conjugated to complex **3** through the formation of the amide bond. The MNP-COOH have amide bonds hence FTIR could not prove definitely that amide bonds were formed between the complex **3** and MNPs. It is expected that the pyridyl groups on the Pc of **3**-MNPs will be quaternized to form **4**-MNPs. The quaternization was confirmed using XPS below.

Scheme 3 represents a hypothetical representation of the **3**- and **4**-MNPs conjugates. There is only one amino group on complex **3**, hence only one point of attachment to the MNPs. Thus, it is not possible for more than one MNP to be attached to complex **3**. It is possible for more than one Pc to link to the MNP. The number of complex **3** molecules bonded to the MNPs was determined following literature methods, but using absorption instead of fluorescence.[43] This involves comparing the Q band absorbance intensity of complex **3** in the conjugate with that of the initial complex **3** before the conjugation. Complex **4**-MNPs was formed from **3**-MNPs hence the number of Pcs will be the same. The ratio of complex **3** to MNPs was found to be 4 : 1.

XRD patterns. The XRD peaks in Fig. 3B, show that MNPs still retain their crystallinity in the conjugates upon formation of an amide bond between the amino group on the photosensitiser and the carboxylic acid group on the nanoparticles, though there is broadening of the peaks.

Thermal analysis. The thermographs (Fig. 6) show weight loss as a function of temperature from 50 to 800 °C. MNP-COOH is more stable than complexes **3** and **4** at all temperatures. Complexes **3** and **4** are less stable than the conjugate (**3**-MNPs) at temperatures less than 500 °C, suggesting that MNPs improve the stability of Pcs below this temperature. The loss in weight could be due to the elimination of adsorbed water, oxidation of any remaining residual organics and relaxation of the silica matrix as the temperature increases.

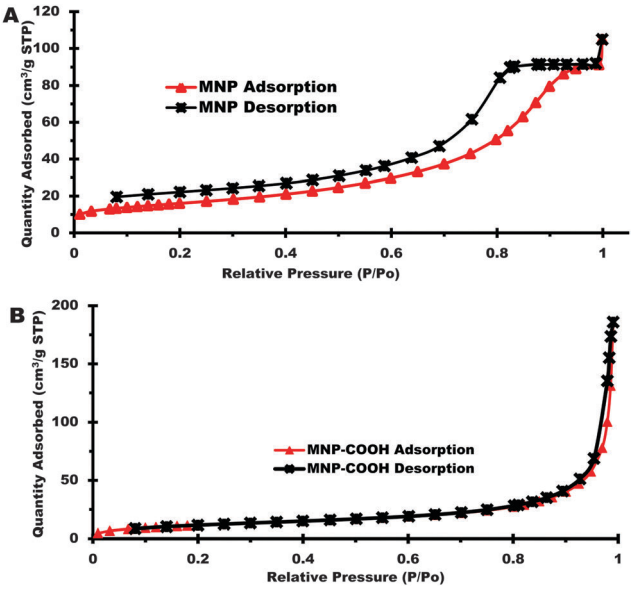

Fig. 4 Typical nitrogen adsorption–desorption BET isotherm of MNP-Si (A) and MNP-COOH (B).

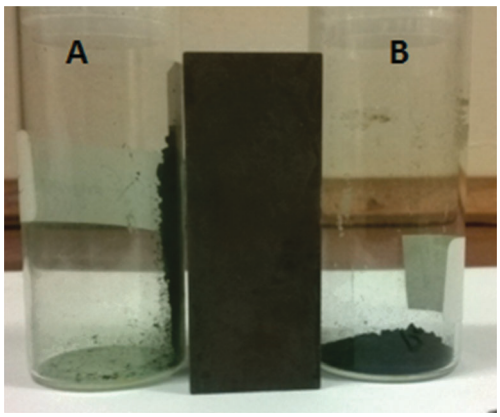

Fig. 5 Photograph of the **3**-MNPs (A) and **3** (B) exhibiting magnetic property of the former.

XPS. The chemical analysis of nanoparticles surface and nanoparticles conjugated with Pcs was carried out using XPS. The survey spectra Fig. 7(A) showed all the expected peaks corresponding to the elements found in Pcs. The expected difference between **3** and **4** is based on the fact that **4** is quartenized (that is the pyridine substituents are positively charged with additional methyl groups), hence the C 1s peak is higher in intensity for **4**. Also complex **4** shows the presence iodide peaks. The chloride peaks are less intense for complex **4**, but they are still present. Fig. 7(B) also shows the spectra of MNP-COOH (blue) and its conjugates with **3** (**3**-MNPs, red) and **4** (**4**-MNPs, black). O 1s, N 1s, C 1s and Si 2p and 2s are from the capping and the core of the NP.

The survey spectra of the conjugates showed (in addition to the MNP-COOH) peaks due to the Pcs (**3** and **4**). The peaks due to Pcs observed in Fig. 7(A) were all prominent in the conjugate.

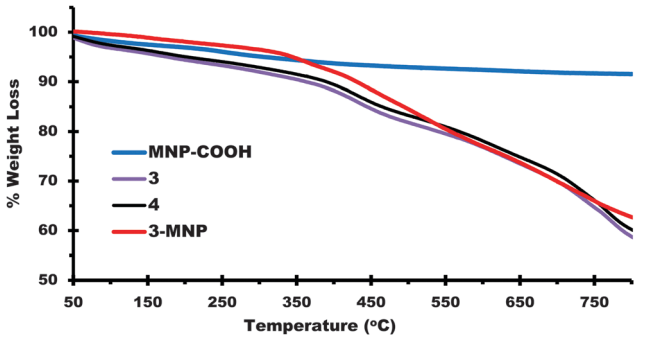

Fig. 6 TGA thermogravimetry of complexes MNP-COOH, **3**, **4** and **3**-MNP.

The increase in relative intensity of N atoms for **3**-MNPs compared to MNP-COOH alone is a result of the presence of N atoms from the Pc. Again, for **4**-MNPs, there is an increase in C peaks due to the presence of the methyl groups. Also the iodide peaks are evident for **4**-MNPs.

To further prove that the nanoparticles are conjugated with Pcs by amide linkage, high resolution N 1s XPS analysis was undertaken. Fig. 8 shows the high resolution N 1s for compound (A) **3**, and (B) **4**. Fig. 8(A) shows the N 1s core level spectrum (for **3**) that could be deconvoluted to show two chemically distinct components centred at 398.7 eV and 400.5 eV and are attributed to N–C and N–H (from NH_2). Upon quaternization of **3** to form **4** the additional peak at 401.6 eV was obtained due to the quaternary nitrogen (N^+), Fig. 8(B). The presence of NH peaks in **4** proves that

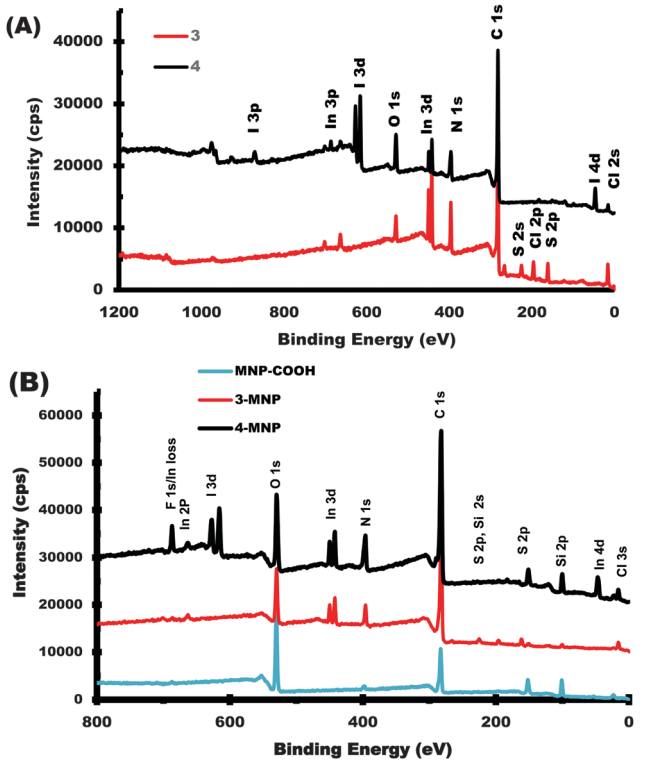

Fig. 7 Survey spectra of (A) **3** (black) and **4** (red), and (B) MNP-NH_2 (blue), **3**-MNPs (black) and **4**-MNPs (red).

the NH_2 group was not quarternized as discussed above. The N1s high resolution peak for the MNP-COOH (Fig. S6B, ESI†), was deconvoluted to yield three components at 398.9 eV, 400.5 eV and 401.9 eV corresponding to N–C, N–H and N–C═O, respectively. The component at high binding energy 401.9 eV due to N–C═O (is an amide bond) between the amino functionalized nanoparticle and the succinic anhydride. This peak is not present in MNP-NH_2 (Fig. S6A, ESI†). The N 1s core level spectra for **3**-MNPs (Fig. 8C) could be fitted into three chemically distinct components with binding energies 398.6 eV, 399.9 eV and 401.7 eV due to (N–C), (N–H) and (N–C═O) bonds, respectively. The higher binding energy component at 401.7 eV corresponds to the amide bond,[40] which further proves that conjugation took place between the MNP-COOH nanoparticles and complex **3**. The amide bond peak is also present in MNP-COOH alone (which has amide bonds, but at different energies). The intensity of the N–C═O peak in Fig. 8C (for the conjugate containing two amide bonds) is larger than that for MNP-COOH (Fig. S6B, ESI† compare the magnitude of the *y* axis units).

In Fig. 8(D), the N 1s core level spectra for **4**-MNPs could be deconvoluted into three chemically distinct components which correspond (N–C), (N–H) and (N–C═O and N^+) groups with binding energies 398.5 eV, 399.9 eV and 401.6 eV; respectively. The higher binding energy component at 401.6 eV corresponds to the amide linkage[44] and quartenized (N^+). This confirms successful quaternization of **3**-MNPs to **4**-MNPs.

The high resolution XPS spectra (for **4**-MNPs) of I 3d was deconvoluted to produce three peaks for I $3d_{5/2}$ and I $3d_{3/2}$ (Fig. 9). The I $3d_{5/2}$ three peaks were observed at 618.79, 620.99 and 622.29 eV whilst the corresponding split orbit coupling peaks for I $3d_{3/2}$ were observed at higher binding energies 630.49, 632.49 and 633.99 eV. The split orbit component separation (ΔE) ranged between 11.2 to 11.5 eV for all the identified components. The three components are due to different iodine chemical binding on the Pc. The first peak at 618.79 eV for I $3d_{5/2}$, is due to the counter anion I^- for quarternized substituents, the second peak at 620.99 eV is due to InCl axial ligand. The small component at higher binding energies 622.69 eV is due to the IO_4^- possibly due to iodine reacting with oxides in solution. The presence of several species of iodine confirmed the successful quaternization of the MPc (**4**).

Fig. S7A and B (ESI†) shows the In 3d spectra of **3**, **3**-MNPs and **4**, **4**-MNPs; respectively. In 3d components could be resolved into two peaks with binding energies of 443.10 and 450.60 eV for **3**-MNPs and 444.41 and 451.99 for **4**-MNP, which are attributed to In $3d_{5/2}$ and $3d_{3/2}$, respectively in trivalent indium ion. This further confirms the presence of In^{3+} within the phthalocyanine rings.[45]

Photophysical and photochemical parameters

Fluorescence quantum yields (Φ_F) and lifetimes (τ_F). Fluorescence quantum yields (Φ_F) were determined by the comparative method described before[46,47] and using ZnPc in DMSO as a standard (Φ_F of standard = 0.20).[47] The fluorescence quantum yields of the photosensitizers were generally low (Table 1) which is a typical behaviour for In central atom (a heavy atom), which encourages intersystem crossing to the triplet state, reducing the amount of fluorescence. For **3**-MNPs, Φ_F value slightly increased compared to **3** alone. However, a decrease would have been expected due to the heavy atom effect

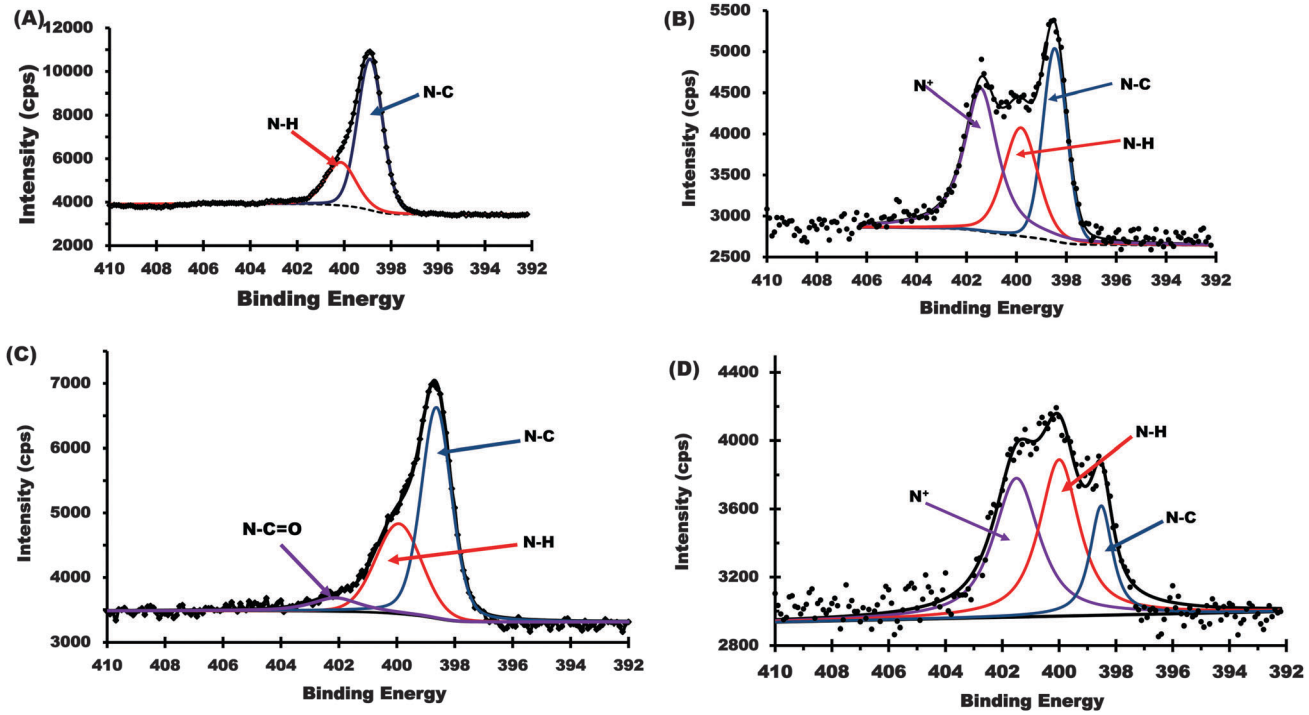

Fig. 8 High resolution of N 1s for (A) **3**, (B) **4**, (C) **3**-MNPs and (D) **4**-MNPs.

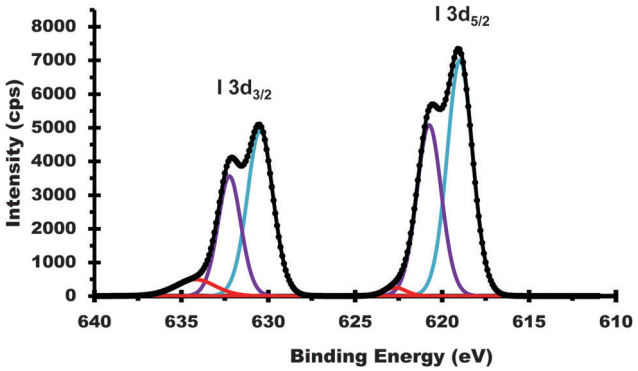

Fig. 9 High resolution of I $3d_{5/2}$ for **4**-MNP.

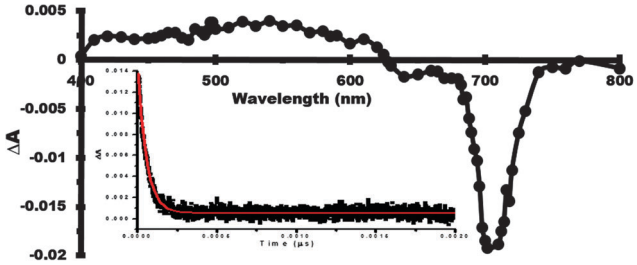

Fig. 10 Transient differential spectrum of complex **3**, excitation wavelength at 680 nm. Inset = corresponding triplet decay curve. Solvent = DMSO.

of the MNPs. For **4**-MNPs, the Φ_F value decreased as expected compared to complex **4** alone in DMSO. This could probably be due to the additional heavy atom effect of iodine in **4** which is not present in **3**. It has been reported that even though the MNP core normally quenches the porphyrin fluorescence, covalent bonding of porphyrin to magnetite nanoparticles *via* an appropriate spacer reduces the quenching.[48] Hence the lack of decrease in the Φ_F value for **3**-MNPs compared to **3** may be a result of the long spacer between the magnetic nanoparticle core and the Pc in Scheme 3, which could also be the case for **4** and **4**-MNP. However, for **4**-MNP, the presence of iodide following quaternization, results in the quenching of fluorescence through the heavy atom effect of the iodine. The fluorescence lifetimes ranged from 0.24–0.33, Table 1. The fluorescence lifetimes become slightly shorter for both complexes in the presence of MNPs.

Triplet quantum yield (Φ_T) and lifetimes (τ_T). The transient absorption spectra of the complex **3** (as a representative in Fig. 10) were measured in DMSO. Both complexes (alone or in the presence of MNPs) show broad absorption bands from 400 nm to 600 nm with absorption maxima around 550 nm which correspond to triplet–triplet absorption spectra. The triplet quantum yields (Φ_T) were calculated at the absorption maxima using comparative method described before[49,50] and ZnPc in DMSO as a standard (Φ_T for the standard = 0.65[49]) the values obtained ranged from 0.48–0.74.

The Φ_T values for **3** and **4** are 0.74 and 0.48, respectively, and the conjugated complexes (**3**-MNPs and **4**-MNPs) gave 0.53 and 0.69, respectively. There is reduction in the triplet quantum yield upon quaternization of **3** to form **4**. The decrease in Φ_T values on quaternization has been reported before.[51] Linking of MNPs also results in the decrease in Φ_T values when comparing **3** with **3**-MNPs. This corresponds to the observed increase in Φ_F since the two are competing processes. For **4**-MNPs, there is an increase in Φ_T values compared to complex **4** alone, corresponding to the decrease in Φ_F value. These observations are a result of the heavy atom effect of iodine for **4**. The triplet lifetimes (τ_T) values ranged from 55 μs to 67 μs and the values for **3**-MNPs and **4**-MNPs remain the same as for **3** and **4**, respectively.

Singlet oxygen quantum yield (Φ_Δ). The Φ_Δ values were determined using DPBF in DMSO or ADMA in aqueous media (water plus Triton X 100) as singlet oxygen quenchers. Comparative methods reported before were employed using ZnPc as a standard in DMSO (Φ_Δ = 0.67 in DMSO)[49] and AlPcSmix in aqueous media (Φ_Δ = 0.44[52]). The concentrations of DPBF and ADMA were lowered to ~0.3 μmol dm^{-3} for all solutions, to avoid chain reactions. DPBF and ADMA degradation was monitored at ~417 nm and ~378 nm respectively. Φ_Δ values are higher for **3** compared to 4, corresponding to Φ_T values which are larger for the former. Φ_Δ values are higher for **3** compared to **3**-MNPs and increase for **4**-MNPs compared to **4**, Table 1. These changes correspond to the changes in Φ_T values. The Φ_Δ values are related to Φ_T values since singlet oxygen is generated from the triplet state. Carvalho *et al.*[40] observed insignificant changes in the singlet oxygen generating abilities of conjugates of porphyrins with MNPs when compared to porphyrins alone. The values of the fraction of the excited triplet state quenched by ground state molecular oxygen ($S_\Delta = \Phi_\Delta/\Phi_T$) are a reflection of the efficiency of energy transfer from the triplet state of the MPc complexes to the ground state of molecular oxygen. These values were greater than 0.5 except for **4**-MNPs, Table 1. The quantum yield of internal conversion (Φ_{IC}) was obtained using the equation $\Phi_{IC} = 1 - (\Phi_T + \Phi_F)$. This equation assumes that only three processes (fluorescence, intersystem crossing and internal conversion) jointly deactivate the singlet excited states of the Pc complexes. The values increased for **3**-MNPs compared to **3** alone and decreased for **4**-MNPs compared to **4**, Table 1. The lowest value of Φ_{IC} was obtained for **3** which also had the largest Φ_T value.

Photodegradation studies (Φ_{Pd}). Photodegradation is a process where a phthalocyanine is degraded under light irradiation.[49] It can be used to determinate MPcs thermal stability and this is especially important for those molecules intended for use as photocatalyst as well as PACT. For determination of photodegradation quantum yields, eqn (1) was employed:[49]

$$\Phi_{Pd} = \frac{(C_0 - C_t) \cdot V \cdot N_A}{I_{abs} \cdot S \cdot t} \quad (1)$$

where C_0 and C_t in mol dm^{-3} are the concentrations of sample before and after irradiation, respectively. V is the reaction volume; S, the irradiated cell area (2.0 cm^2); t, the irradiation time; N, the Avogadro's number and I_{abs}, the overlap integral of the radiation source intensity and the absorption of the sample in the region of the interference filter transmittance. Both complexes **3** and **4** (and their conjugates) are relatively stable

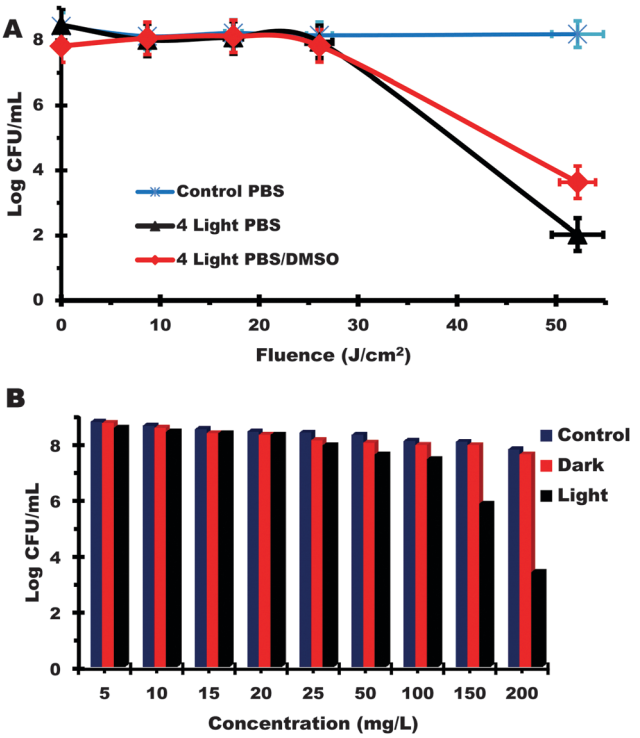

Fig. 11 Photodynamic inactivation efficiency of (A) **4** in PBS and PBS/DMSO and (B) **4**-MNPs on *E. coli* in PBS/DMSO.

in DMSO, Table 1. For unstable complexes, the Φ_{Pd} values are of the order of 10^{-3}.[49] The stability is lower for complex **4** in water plus Triton X 100.

Bacterial studies. As stated above, cationic photosensitizers are more effective hence **3** was not studied for PACT. **4**, **3**-MNPs and **4**-MNPs were studied for PACT even though **3**-MNPs is not cationic. The later was studied for comparative purposes. The inactivation of the bacterial with complex **4** in PBS was carried out at a constant concentration of 10 μM (14 mg L^{-1}) at varying irradiance time (Fig. 11). A log reduction value for *E. coli* of 6.45 (Table 2) was obtained after 60 min (Table 2). The PACT experiments using **3**-MNPs and **4**-MNPs were not as effective at a lower concentration. We were able to achieve a reasonable log CFU per mL with 200 mg L^{-1} for **4**-MNP. The same concentration was used for **3**-MNPs. Carvalho *et al.*[40] also observed what we observe in this work, *i.e.* larger amounts of the nanocomposites were required to achieve a similar antibacterial activity as for the porphyrin alone. The major advantage of using the MNP (as opposed to non-magnetic nanoparticles or Pc alone) together with the photosensitizer is the possibility of removal following use. **4**-MNPs gave an acceptable log reduction which was similar to that of **4** alone within error limits. The non-cationic conjugate (**3**-MNPs) was not effective even at a higher concentrations (log CFU = 0.8). Singlet oxygen is cytotoxic to the targeted bacteria. Singlet oxygen quantum yield values for **4**-MNPs and **3**-MNPs are not too different, Table 1, hence their differences in activity is related to the differences in charge. Fig. 11B shows that the nanoconjugates did not show dark toxicity.

Table 2 Log reduction values for the photoinactivation effect on *E. coli* inactivation

Complexes	Solvents	Concentration (mg L^{-1})	Log reduction
4	PBS	14 (10 mM)	6.45 ± 2.01
	DMSO/PBS	14 (10 mM)	4.90 ± 1.79
3-MNPs	DMSO/PBS	200	0.80 ± 0.03
4-MNPs	DMSO/PBS	200	4.39 ± 1.65

Conclusions

The magnetic nanoparticle (MNP) functionalized with carboxylic acid were linked *via* an amide linkage to the amino group on the metallophthalocyanine (**3**) to form **3**-MNPs, which was quartenized using methyl iodide to give **4**-MNPs. The photosensitisers were characterised and their effectiveness on gram negative (*E. coli*) were studied. The cationic photosensitiser **4**, show a high efficiency at a very low concentration when compared to the quartenized photosensitiser conjugated with the functionalized magnetic nanoparticles. **4**-MNPs gave log reduction which was similar (within experimental error) to that for **4** alone in the same solvent medium. The log reduction values for **4** and **4**-MNP are greater than the accepted log 3 and the latter has the advantage of ease of separation (with a magnet) following use and the low dark toxicity. The results in this work show that the magnitude of singlet oxygen quantum yield is less important than charge in PACT.

Acknowledgements

This work was supported by the department of science and Technology, Republic of South Africa and National Research Foundation through DST/NRF South Africa Research Chairs Initiative for Professor of Medicinal Chemistry and Nanotechnology (Grant number UID 62620) and Rhodes University.

References

1 M. B. Spesia, M. E. Milanesio and E. N. Durantini, *Eur. J. Med. Chem.*, 2008, **43**, 853–861.
2 M. D. R. S. Freire, D. C. Isabele, C. F. Paulo, M. A. C. Maria, F. G. Eduardo and S. A. Viviane, *Arch. Oral Sci. Res.*, 2012, **2**, 88–93.
3 R. Bonnet, *Chemical Aspect of Photodynamic Therapy*, Gordon and Breach, Amsterdam, 2000.
4 H. Ali and J. E. Van Lier, *Tetrahedron Lett.*, 2013, **54**, 2956–2959.
5 M. Wainwright, *J. Antimicrob. Chemother.*, 1998, **42**, 13–28.
6 R. F. Donnelly, P. A. McCarron and M. M. Tunney, *Microbiol. Res.*, 2008, **163**, 1–12.
7 D. Dini, M. J. F. Calvete, M. Hanack and M. Meneghetti, *J. Phys. Chem. A*, 2008, **112**, 8515–8522.
8 F. Dumoulin, M. Durmuş, V. Ahsen and T. Nyokong, *Coord. Chem. Rev.*, 2010, **254**, 2792–2847.
9 S. Z. Topal, Ü. İşci, U. Kumru, D. Atilla, A. G. Gürek, C. Hirel, M. Durmuş, J.-B. Tommasino, D. Luneau, S. Berber, F. Dumoulin and V. Ahsen, *Dalton Trans.*, 2014, **43**, 6897–6908.

10 A. Ito, M. Shinkai, H. Honda and T. Kobayashi, *J. Biosci. Bioeng.*, 2005, **100**, 1–11.
11 S. A. Corr, Y. P. Rakovich and Y. K. Gun'ko, *Nanoscale Res. Lett.*, 2008, **3**, 87–104.
12 H. Bin Na, I. C. Song and T. Hyeon, *Adv. Mater.*, 2009, **21**, 2133–2148.
13 J. Chomoucka, J. Drbohlavova, D. Huska, V. Adam, R. Kizek and J. Hubalek, *Pharmacol. Res.*, 2010, **62**, 144–149.
14 E. Cheraghipour, S. Javadpour and A. R. Mehdizadeh, *J. Biomed. Sci. Eng.*, 2012, **5**, 715–719.
15 Y. H. Deng, C. C. Wang, J. H. Hu, W. L. Yang and S. K. Fu, *Colloids Surf., A*, 2005, **262**, 87–93.
16 T. Nann, *Nano Biomed. Eng.*, 2011, **3**, 137–143.
17 B. Gottenbos, *J. Antimicrob. Chemother.*, 2001, **48**, 7–13.
18 T. Nyokong and H. Isago, *J. Porphyrins Phthalocyanines*, 2004, **8**, 1083–1090.
19 N. Masilela, P. Kleyi, Z. Tshentu, G. Priniotakis, P. Westbroek and T. Nyokong, *Dyes Pigm.*, 2013, **96**, 500–508.
20 O. L. Osifeko, M. Durmus and T. Nyokong, *J. Photochem. Photobiol., A*, 2015, **301**, 47–54.
21 N. Masilela and T. Nyokong, *J. Photochem. Photobiol., A*, 2013, **255**, 1–9.
22 N. Nombona, E. Antunes, W. Chidawanyika, P. Kleyi, Z. Tshentu and T. Nyokong, *J. Photochem. Photobiol., A*, 2012, **233**, 24–33.
23 A. R. Simioni, M. M. a Rodrigues, F. L. Primo, P. C. Morais and A. C. Tedesco, *J. Nanosci. Nanotechnol.*, 2011, **11**, 3604–3608.
24 P. Modisha, E. Antunes, J. Mack and T. Nyokong, *Int. J. Nanosci.*, 2013, **12**, 1350010.
25 F. L. Primo, M. M. A. Rodrigues, A. R. Simioni, Z. G. M. Lacava, P. C. Morais and A. C. Tedesco, *J. Nanosci. Nanotechnol.*, 2008, **8**, 5873–5877.
26 S. D'Souza, E. Antunes and T. Nyokong, *Inorg. Chim. Acta*, 2011, **367**, 173–181.
27 K. Sanusi, E. K. Amuhaya and T. Nyokong, *J. Phys. Chem. C*, 2014, **118**, 7057–7069.
28 T. Teixeira Tasso, Y. Yamasaki, T. Furuyama and N. Kobayashi, *Dalton Trans.*, 2014, **43**, 5886–5892.
29 M. Ambroz, A. Beeby, A. J. MacRobert, M. S. Simpson, R. K. Svensen and D. Phillips, *J. Photochem. Photobiol., B*, 1991, **9**, 87–95.
30 A. Fashina, E. Antunes and T. Nyokong, *Polyhedron*, 2013, **53**, 278–285.
31 I. Scalise and E. N. Durantini, *Bioorg. Med. Chem.*, 2005, **13**, 3037–3045.
32 V. Mantareva, V. Kussovski, I. Angelov, E. Borisova, L. Avramov, G. Schnurpfeil and D. Wöhrle, *Bioorg. Med. Chem.*, 2007, **15**, 4829–4835.
33 V. Kussovski, V. Mantareva, I. Angelov, P. Orozova, D. Wohrle, G. Schnurpfeil, E. Borisova and L. Avramov, *FEMS Microbiol. Lett.*, 2009, **294**, 133–140.
34 B. D. Jett, K. L. Hatter, M. M. Huycke and M. S. Gilmore, *Biotechniques*, 1997, **23**, 648–650.
35 T. Kiesslich, A. Gollmer, T. Maisch, M. Berneburg and K. Plaetzer, *BioMed Res. Int.*, 2013, 1–17.
36 T. N. Demidova and M. R. Hamblin, *Antimicrob. Agents Chemother.*, 2005, **49**, 2329–2335.
37 Z. Ma, X. Liu, Y. Guan and H. Liu, *Colloids Surf., A*, 2006, **275**, 87–91.
38 X. Liu, Z. Ma, J. Xing and H. Liu, *J. Magn. Magn. Mater.*, 2004, **270**, 1–6.
39 K. Sanusi, J. M. Stone and T. Nyokong, *New J. Chem.*, 2015, **39**, 1665–1677.
40 C. M. B. Carvalho, E. Alves, L. Costa, J. P. C. Tome, M. A. F. Faustino, M. G. P. M. S. Neves, A. C. Tome, J. A. S. Cavaleiro, A. Almeida, A. Cunha, Z. Lin and J. Rocha, *ACS Nano*, 2010, **12**, 7133–7140.
41 M. Sibrian-Vazquez J. Ortiz, I. V. Nesterova, F. Fernández-Lázaro, A. Sastre-Santos, S. A. Soper and M. G. H. Vicente, *Bioconjugate Chem.*, 2007, **18**, 410–420.
42 S. Xu, S. Hartvickson and J. X. Zhao, *ACS Appl. Mater. Interfaces*, 2011, **3**, 1865–1872.
43 L. Li, J.-F. Zhao, N. Won, H. Jin, S. Kim and J.-Y. Chen, *Nanoscale Res. Lett.*, 2012, **7**, 386.
44 T. Ramanathan, F. T. Fisher, R. S. Ruoff and L. C. Brinson, *Chem. Mater.*, 2005, **17**, 1290–1295.
45 R. W. Hewitt and N. Winograd, *J. Appl. Phys.*, 1980, **51**, 2620–2624.
46 S. Fery-Forgues and D. Lavabre, *J. Chem. Educ.*, 1999, **76**, 1260–1264.
47 A. Ogunsipe, J. Chen and T. Nyokong, *New J. Chem.*, 2004, **28**, 822–827.
48 S. A. Corr, A. O' Byrne, Y. K. Gun'ko, S. Ghosh, D. F. Brougham, S. Mitchell, Y. Volkov and A. Prina-Mello, *Chem. Commun.*, 2006, 4474–4476.
49 T. Nyokong and E. Antunes, in *In the handbook of porphyrin science*, ed. K. M. Kadish, K. M. Smith and R. Guilard, Academic Press, New York, 2010, vol. 7, pp. 247–349.
50 T. H. Tran Thi, C. Desforge, C. Thiec and S. Gaspard, *J. Phys. Chem.*, 1989, **93**, 1226–1233.
51 S. Moeno and T. Nyokong, *J. Photochem. Photobiol., A*, 2010, **215**, 196–204.
52 A. Ogunsipe and T. Nyokong, *Photochem. Photobiol. Sci.*, 2005, **4**, 510–516.